

Approximate analytical solutions of the Bidomain equations for electrical stimulation of cardiac tissue with curving fibers

Bradley J. Roth and Deborah Langrill Beaudoin

Department of Physics, Oakland University, Rochester, Michigan 48309

(Received 8 November 2002; published 27 May 2003)

The mechanism by which an applied electric field stimulates cardiac tissue far from the stimulating electrodes is not wholly understood. One possible mechanism relates the curving cardiac fibers to the induced membrane currents and transmembrane potentials. However, we lack a qualitative understanding of where these areas of polarization will occur when an electric field is applied to a sheet of cardiac tissue with curving fibers. In our study, we derive an analytical model for the transmembrane potential, dependent on the gradient of the fiber angle θ , for a two-dimensional passive sheet of cardiac tissue exhibiting various fiber geometries. Unequal anisotropy ratios are crucial for our results. We compare the results from our analytical solution to a numerical calculation using the full bidomain model. The results of our comparison are qualitatively consistent, albeit numerically different. We believe that our analytical approximation provides a reliable prediction of the polarization associated with an electric field applied to cardiac tissue with any fiber geometry and a qualitative understanding of the mechanisms behind the virtual electrode polarization.

DOI: 10.1103/PhysRevE.67.051925

PACS number(s): 87.19.Hh, 87.18.-h, 87.10.+e, 87.90.+y

I. INTRODUCTION

The mechanism for electrical stimulation of cardiac tissue has been studied intensely over the past few years [1]. This is an important topic because of the role electrical stimulation plays in cardiac pacing and defibrillation. Of particular interest is “far-field” stimulation, which we take to mean excitation of cardiac tissue far from any stimulating electrode or tissue boundary. One proposed mechanism for far-field stimulation is based on “fiber curvature” [2,3]. According to this hypothesis, when an electric field is applied to the tissue the change in the direction of the myocardial fibers with position induces membrane currents and a transmembrane potential. Although this mechanism has been studied extensively in numerical simulations [4–6], we still lack a qualitative understanding of how it works. If the fiber direction in the x - y plane is specified by $\theta(x,y)$, the angle between the fibers and the x axis, we have found it difficult to predict which regions of the tissue will be polarized by an electric field simply by inspection of $\theta(x,y)$. For example, Fig. 1 shows the fiber geometry throughout a sheet of tissue and the direction of the applied electric field. Can you look at Fig. 1 and predict where the tissue will be depolarized and where it will be hyperpolarized? Our goal in this paper is to elucidate the mechanism of tissue polarization caused by fiber curvature, and to provide a way to predict the distribution of polarization qualitatively.

II. DERIVATION OF THE ANALYTICAL EQUATIONS

We represent cardiac tissue using the bidomain model [7], which accounts for both the intracellular and extracellular spaces. In a two-dimensional sheet of tissue, the local properties of the anisotropic bidomain are governed by five parameters: the intracellular conductivity parallel to the fibers, g_{iL} ; the intracellular conductivity perpendicular to the fibers, g_{iT} ; the extracellular conductivity parallel to the fibers, g_{eL} ; the extracellular conductivity perpendicular to the fibers, g_{eT} ;

and the local fiber direction, $\theta(x,y)$. The values of the four bidomain conductivities are fairly well known [8], and we assume they are the same everywhere. In general, the fiber direction is not fixed, but varies throughout the tissue.

We can write the four bidomain conductivities in terms of four more useful parameters: $g_L = g_{iL} + g_{eL}$, $g_T = g_{iT} + g_{eT}$, $\alpha = g_{iL}/g_{eL}$, and $e = 1 - [(g_{eL}/g_{eT})/(g_{iL}/g_{iT})]$. These parameters are similar to the ones used in [8], except that for far-field stimulation the parallel combinations of conductivities, g_L and g_T , are more convenient to work with than the series combinations in [8]. The parameter e is particularly useful, because it is equal to zero when the tissue has “equal anisotropy ratios” ($g_{eL}/g_{eT} = g_{iL}/g_{iT}$). We can write the four bidomain conductivities in terms of these parameters as

$$g_{iL} = g_L \left(\frac{\alpha}{1 + \alpha} \right), \quad (1)$$

$$g_{iT} = g_T \left(\frac{\alpha(1 - e)}{1 + \alpha(1 - e)} \right), \quad (2)$$

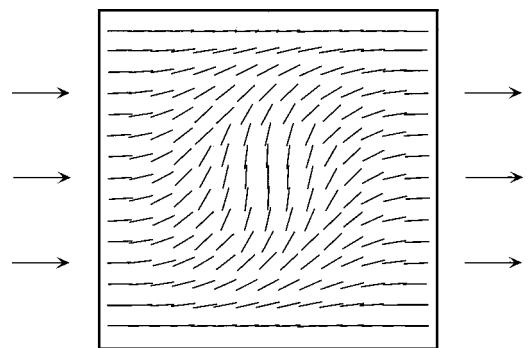


FIG. 1. The line segments indicate the fiber direction in a two-dimensional sheet of cardiac tissue, and the arrows indicate the direction of the applied electric field. The reader’s task is to predict qualitatively the resulting transmembrane potential distribution.

$$g_{eL} = g_L \left(\frac{1}{1 + \alpha} \right), \quad (3)$$

$$g_{eT} = g_T \left(\frac{1}{1 + \alpha(1 - e)} \right). \quad (4)$$

In a fixed Cartesian coordinate system (x, y) , the fiber direction does not generally align with the coordinate axes. Therefore, both the intracellular and extracellular conductivity tensors are functions of position [through the fiber angle $\theta(x, y)$] and will in general have off-diagonal components [9]

$$\tilde{g} = \begin{pmatrix} g_L \cos^2 \theta + g_T \sin^2 \theta & (g_L - g_T) \cos \theta \sin \theta \\ (g_L - g_T) \cos \theta \sin \theta & g_L \sin^2 \theta + g_T \cos^2 \theta \end{pmatrix}. \quad (5)$$

The bidomain equations govern the intracellular potential V_i and the extracellular potential V_e ,

$$\nabla \cdot \tilde{g}_i \nabla V_i = \beta G_m (V_i - V_e), \quad (6)$$

$$\nabla \cdot \tilde{g}_e \nabla V_e = -\beta G_m (V_i - V_e), \quad (7)$$

where β is the ratio of membrane surface area to tissue volume and G_m is the membrane conductance per unit area. These equations are based on the assumption that the tissue is in steady state, and that the membrane is passive. Previously, we found that the bidomain equations are easier to analyze analytically when written in terms of two different potentials, V_m and ψ , which are linear combinations of V_i and V_e

$$V_m = V_i - V_e, \quad (8)$$

$$\psi = V_i + \frac{1}{\alpha} V_e, \quad (9)$$

where V_m is the transmembrane potential and ψ is an auxiliary potential with no simple physical interpretation [10]. We can invert these relationships to determine V_i and V_e in terms of V_m and ψ

$$V_i = \frac{\alpha}{1 + \alpha} \left(\psi + \frac{1}{\alpha} V_m \right), \quad (10)$$

$$V_e = \frac{\alpha}{1 + \alpha} (\psi - V_m). \quad (11)$$

If we add Eqs. (6) and (7) and express them in terms of V_m and ψ , we obtain

$$\nabla \cdot (\tilde{g}_i + \tilde{g}_e) \nabla \psi = -\nabla \cdot \left(\tilde{g}_i \frac{1}{\alpha} - \tilde{g}_e \right) \nabla V_m. \quad (12)$$

If we multiply Eq. (6) by g_{iT}/g_{eT} , and subtract the product from Eq. (7), we get

$$\begin{aligned} \nabla \cdot \left(\tilde{g}_i \frac{1}{\alpha} + \alpha(1 - e) \tilde{g}_e \right) \nabla V_m - \frac{1 + \alpha}{\alpha} \beta G_m [1 + \alpha(1 - e)] V_m \\ = -\nabla \cdot [\tilde{g}_i - \alpha(1 - e) \tilde{g}_e] \nabla \psi. \end{aligned} \quad (13)$$

Equations (12) and (13) are two coupled partial differential equations that need to be solved for V_m and ψ . Analytical solutions to these equations are rare, except in the case of equal anisotropy ratios. Therefore, we search for approximate analytical solutions using a perturbative expansion in powers of e , with the zeroth order term in this expansion corresponding to equal anisotropy ratios. This type of expansion proved useful for analyzing unipolar stimulation of cardiac tissue and for understanding the extracellular potential produced by an expanding wave front [10].

To begin, we expand V_m and ψ in powers of e

$$V_m = V_{m0} + e V_{m1} + e^2 V_{m2} + \dots, \quad (14)$$

$$\psi = \psi_0 + e \psi_1 + e^2 \psi_2 + \dots. \quad (15)$$

We can also expand the expressions for the bidomain conductivities [Eqs. (1)–(4)] in powers of e . Placing these expressions into Eqs. (12) and (13), we collect terms with common powers of e to obtain equations governing V_{m0} , ψ_0 , V_{m1} , etc.

The zeroth-order equation for ψ_0 is

$$\begin{aligned} \frac{\partial}{\partial x} \left[(g_L \cos^2 \theta + g_T \sin^2 \theta) \frac{\partial \psi_0}{\partial x} + (g_L - g_T) \cos \theta \sin \theta \frac{\partial \psi_0}{\partial y} \right] \\ + \frac{\partial}{\partial y} \left[(g_L - g_T) \cos \theta \sin \theta \frac{\partial \psi_0}{\partial x} \right. \\ \left. + (g_L \sin^2 \theta + g_T \cos^2 \theta) \frac{\partial \psi_0}{\partial y} \right] = 0. \end{aligned} \quad (16)$$

This boundary value problem for ψ_0 does not depend on V_m (the equations uncouple for $e=0$). This expression is difficult to solve when the tissue is anisotropic, $g_L \neq g_T$, with an arbitrary fiber geometry $\theta(x, y)$. When $g_L = g_T$, Eq. (16) reduces to Laplace's equation, $\nabla^2 \psi_0 = 0$. The solution depends on the boundary conditions for ψ_0 . In this paper, we are concerned with boundary conditions that correspond to a uniform electric field at large $|x|$ and $|y|$.

The zeroth-order equation for V_{m0} is

$$\begin{aligned} \frac{\partial}{\partial x} \left[(g_L \cos^2 \theta + g_T \sin^2 \theta) \frac{\partial V_{m0}}{\partial x} \right. \\ \left. + (g_L - g_T) \cos \theta \sin \theta \frac{\partial V_{m0}}{\partial y} \right] \\ + \frac{\partial}{\partial y} \left[(g_L - g_T) \cos \theta \sin \theta \frac{\partial V_{m0}}{\partial x} \right. \\ \left. + (g_L \sin^2 \theta + g_T \cos^2 \theta) \frac{\partial V_{m0}}{\partial y} \right] - \frac{g_L}{\lambda_L^2} V_{m0} = 0, \end{aligned} \quad (17)$$

where the length constant λ_L is equal to $\sqrt{g_{iL}g_{eL}/(g_{iL}+g_{eL})\beta G_m}$. This equation does not depend on ψ_0 . When $g_L = g_T$, it reduces to the two-dimensional cable equation, $\nabla^2 V_{m0} - V_{m0}/\lambda_L^2 = 0$. If we assume that V_{m0} goes to zero at large $|x|$ and $|y|$, then the solution to this equation is $V_{m0} = 0$. There is no transmembrane potential induced in the case of equal anisotropy ratios.

To determine the first nonzero contribution to the transmembrane potential, we consider the first-order equation for V_{m1}

$$\begin{aligned} & \frac{\partial}{\partial x} \left[(g_L \cos^2 \theta + g_T \sin^2 \theta) \frac{\partial V_{m1}}{\partial x} + (g_L - g_T) \right. \\ & \quad \times \cos \theta \sin \theta \frac{\partial V_{m1}}{\partial y} \left. \right] + \frac{\partial}{\partial y} \left[(g_L - g_T) \cos \theta \sin \theta \frac{\partial V_{m1}}{\partial x} \right. \\ & \quad \left. + (g_L \sin^2 \theta + g_T \cos^2 \theta) \frac{\partial V_{m1}}{\partial y} \right] - \frac{g_L}{\lambda_L^2} V_{m1} \\ & = -g_L \frac{\alpha}{1+\alpha} \left\{ \frac{\partial}{\partial x} \left[\cos^2 \theta \frac{\partial \psi_0}{\partial x} + \cos \theta \sin \theta \frac{\partial \psi_0}{\partial y} \right] \right. \\ & \quad \left. + \frac{\partial}{\partial y} \left[\cos \theta \sin \theta \frac{\partial \psi_0}{\partial x} + \sin^2 \theta \frac{\partial \psi_0}{\partial y} \right] \right\}. \end{aligned} \quad (18)$$

Although this equation appears formidable, in many cases the fiber geometry is smooth, so that $\theta(x,y)$ changes little over distances on the order of the length constant λ_L . In that case, the first two terms on the left-hand side of Eq. (18) are negligible compared to the third, and Eq. (18) becomes simply

$$\begin{aligned} V_{m1} = & \lambda_L^2 \frac{\alpha}{1+\alpha} \left\{ \frac{\partial}{\partial x} \left[\cos^2 \theta \frac{\partial \psi_0}{\partial x} + \cos \theta \sin \theta \frac{\partial \psi_0}{\partial y} \right] \right. \\ & \left. + \frac{\partial}{\partial y} \left[\cos \theta \sin \theta \frac{\partial \psi_0}{\partial x} + \sin^2 \theta \frac{\partial \psi_0}{\partial y} \right] \right\}. \end{aligned} \quad (19)$$

This is our central result. In the literature on bioelectric phenomena, the expression on the right-hand-side of Eq. (19) is called the ‘‘activating function.’’

To make further progress, we must know ψ_0 . But ψ_0 is difficult to determine in general; we must solve Eq. (16). We can make initial progress understanding the physical basis of far field stimulation if we assume $g_L = g_T$ so that ψ_0 obeys Laplace’s equation. The simplest solution of Laplace’s equation is a uniform electric field of strength E_0 in the direction ϕ :

$$\psi_0 = -\frac{1+\alpha}{\alpha} E_0 (x \cos \phi + y \sin \phi). \quad (20)$$

The factor of $(1+\alpha)/\alpha$ ensures that when ψ_0 is substituted into Eqs. (10) and (11), the strength of the electric field in both the intracellular and extracellular spaces is E_0 . Substituting Eq. (20) into Eq. (19), and taking the derivatives of the trigonometric functions, we find that

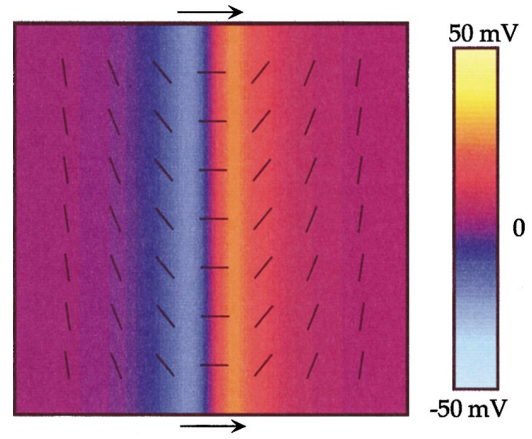


FIG. 2. (Color) The transmembrane potential as a function of x (horizontal) and y (vertical). The fiber geometry is given by $\theta(x,y) = \tan^{-1}(x/L)$, and the local fiber direction is indicated by the line segments. A 20×20 mm² region of tissue is shown, with the origin at the center. The arrows indicate that the electric field points to the right (x direction). The parameters used in this calculation are $E_0 = 500$ V/m, $\phi = 0$, $\lambda_L = 0.434$ mm, $e = 0.75$, and $L = 2$ mm.

$$\begin{aligned} V_{m1} = & E_0 \lambda_L^2 \left[\cos \phi \left(\sin 2\theta \frac{\partial \theta}{\partial x} - \cos 2\theta \frac{\partial \theta}{\partial y} \right) \right. \\ & \left. + \sin \phi \left(-\cos 2\theta \frac{\partial \theta}{\partial x} - \sin 2\theta \frac{\partial \theta}{\partial y} \right) \right], \end{aligned} \quad (21)$$

or, in a somewhat more compact form,

$$V_{m1} = \lambda_L^2 \vec{E}_0 \cdot \tilde{D} \cdot \vec{\nabla} \theta, \quad (22)$$

where

$$\tilde{D} = \begin{pmatrix} \sin 2\theta & -\cos 2\theta \\ -\cos 2\theta & -\sin 2\theta \end{pmatrix}. \quad (23)$$

III. SIMPLE EXAMPLES

As a first example, consider a fiber geometry similar to that examined by Skouibine *et al.* [5],

$$\theta(x,y) = \tan^{-1} \left(\frac{x}{L} \right), \quad (24)$$

shown in Fig. 2. In this case,

$$\sin 2\theta = \frac{2xL}{L^2 + x^2}, \quad (25)$$

$$\cos 2\theta = \frac{L^2 - x^2}{L^2 + x^2}, \quad (26)$$

$$\frac{\partial \theta}{\partial x} = \frac{L}{L^2 + x^2}, \quad (27)$$

and

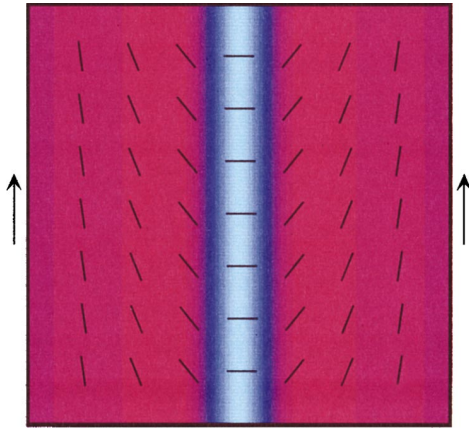


FIG. 3. (Color) The transmembrane potential as a function of x (horizontal) and y (vertical). The fiber geometry is given by $\theta(x,y) = \tan^{-1}(x/L)$, and the local fiber direction is indicated by the line segments. A $20 \times 20 \text{ mm}^2$ region of tissue is shown, with the origin at the center. The arrows indicate that the electric field points up (y direction). The parameters used in this calculation are $E_0 = 500 \text{ V/m}$, $\phi = \pi/2$, $\lambda_L = 0.434 \text{ mm}$, $e = 0.75$, and $L = 2 \text{ mm}$. The color bar is the same as in Fig. 2.

$$\frac{\partial \theta}{\partial y} = 0, \tag{28}$$

so

$$V_m = \frac{eE_0\lambda_L^2}{L} \frac{1}{\left[1 + \left(\frac{x}{L}\right)^2\right]^{3/2}} \left\{ \cos \phi \frac{x}{L} - \sin \phi \left[1 - \left(\frac{x}{L}\right)^2\right]\right\}, \tag{29}$$

correct to first order in powers of e . Figure 2 shows a plot of V_m when the electric field is in the x direction ($E_0 = 500 \text{ V/m}$, $\phi = 0$, $\lambda_L = 0.434 \text{ mm}$, $e = 0.75$, and $L = 2 \text{ mm}$). The transmembrane potential is negative (hyperpolarized) on the left (minimum = -23 mV), and positive (depolarized) on the right (maximum = 23 mV). Figure 3 shows a similar plot for the electric field in the y direction ($\phi = \pi/2$). The transmembrane potential is strongly hyperpolarized in the center (minimum = -35 mV), and weakly depolarized to the left and right (maximum = 4 mV).

This simple example is useful because it highlights the two mechanisms underlying the polarization of cardiac tissue by an applied electric field when fibers curve. Figure 4(a) shows schematically the first mechanism, which applies when the fiber orientation changes along the direction parallel to the electric field [the first term in Eq. (29)]. On the left, the electric field E is parallel to the fibers. In this case, the intracellular and extracellular conductivities are similar ($g_{iL} = g_{eL}$) [8], and the net current density J divides evenly between J_i and J_e , the current densities in the intracellular and extracellular spaces. On the right, the electric field is perpendicular to the fibers. In this case, the intracellular conductivity is much less than the extracellular conductivity, $g_{iT} < g_{eT}$ [8]. Therefore, J (which is the same on the left and right, because we are assuming $g_L = g_T$) flows primarily in

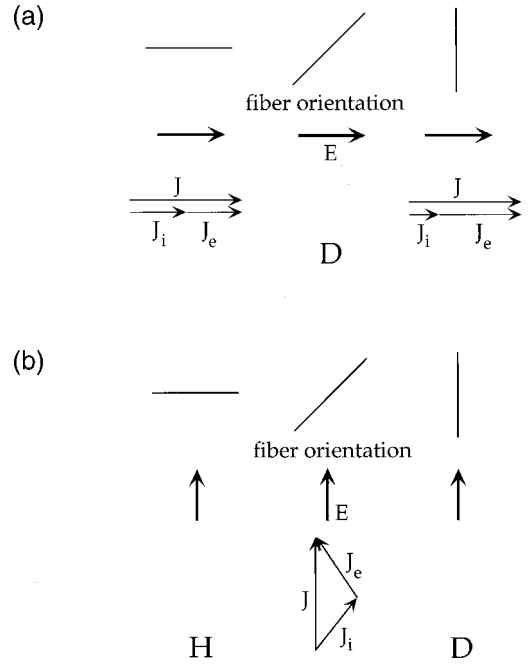


FIG. 4. A schematic diagram illustrating the mechanisms of far-field electrical stimulation due to fiber curvature. (a) First mechanism, when the fiber orientation changes in the direction parallel to the electric field. (b) Second mechanism, when the fiber orientation changes in the direction perpendicular to the electric field.

the extracellular space, with relatively little current passing through the more resistive intracellular space. As the fiber orientation changes from parallel to perpendicular to the electric field (middle), current redistributes from the intracellular space into the extracellular space, which depolarizes the membrane (D). Similarly, if the fiber orientation changes from perpendicular to parallel to the electric field, current redistributes from the extracellular into the intracellular space, hyperpolarizing the membrane. This behavior is consistent with the transmembrane potential distribution shown in Fig. 2. Note that unequal anisotropy ratios are crucial for this mechanism. If g_{iL}/g_{eL} is the same as g_{iT}/g_{eT} , the ratio of intracellular to extracellular current is the same regardless of the fiber orientation, so there is no current redistribution between the intracellular and extracellular spaces, and no membrane polarization. Only when $g_{iL}/g_{eL} \neq g_{iT}/g_{eT}$ (or, equivalently, $g_{iL}/g_{iT} \neq g_{eL}/g_{eT}$) is V_m nonzero. This mechanism has been described before (see Fig. 10 of [1]).

The second term in Eq. (29) corresponds to the fiber orientation changing along the direction perpendicular to the electric field. We have never seen this second mechanism described in the literature, but it appears to be as important as the first mechanism. Figure 4(b) elucidates this second mechanism. When the electric field is either perpendicular to (left) or parallel to (right) the fiber direction, J , J_i , and J_e are all in the same direction as the electric field. When the electric field is at an angle to the fiber direction (middle), the net current J is parallel to E because $g_L = g_T$. However, J_i and J_e individually have components perpendicular to the elec-

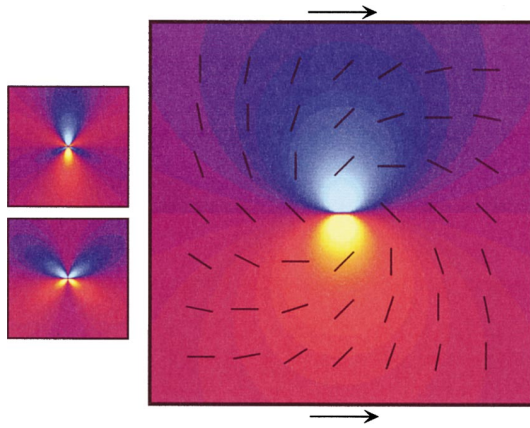


FIG. 5. (Color) The transmembrane potential as a function of x (horizontal) and y (vertical). The fiber geometry is given by $\theta(x,y) = \tan^{-1}(y/x) + 3\pi/4$, and the local fiber direction is indicated by the line segments. A 20×20 mm² region of tissue is shown, with the origin at the center. The arrows indicate that the electric field points to the right (x direction). The parameters used in this calculation are $E_0 = 500$ V/m, $\phi = 0$, $\lambda_L = 0.434$ mm, and $e = 0.75$. The two small panels on the left indicate the separate contributions of the two mechanisms. The color bar is the same as in Fig. 2.

tric field.¹ This results in a current loop: intracellular current flows to the right, where it exits the intracellular space and depolarizes the tissue (D), and then returns as extracellular current to the left, where it enters the intracellular space and hyperpolarizes the tissue (H). If the anisotropy ratios were equal, both J_i and J_e would individually be parallel to E , and the current loop and transmembrane polarization would disappear. This behavior is consistent with the transmembrane potential distribution shown in Fig. 3. This mechanism is analogous to the one responsible for tissue polarization when the fibers approach a sealed boundary in the presence of an electric field [11].

Both of these mechanisms are particularly clear when we assume $g_L = g_T$. Of course in cardiac tissue this is not the case; g_L is about 4 times larger than g_T [8]. This complicates the calculation of ψ_0 and implies that the electric field varies throughout the tissue. But the underlying mechanisms remain the same.

Another simple fiber geometry, shown in Fig. 5, is reminiscent of that present at the apex of the heart [12]

¹That J_e rotates away from the fiber direction is a consequence of our unrealistic assumption that $g_L = g_T$. For instance, the parameters $g_L = g_T = 0.4$ S/m, $\alpha = 1$, and $e = 0.75$ correspond to the conductivities $g_{iL} = 0.2$ S/m, $g_{iT} = 0.08$ S/m, $g_{eL} = 0.2$ S/m, and $g_{eT} = 0.32$ S/m. In this case, the extracellular space has its largest conductivity perpendicular to the fibers. In real cardiac tissue, $g_L \neq g_T$, and both the intracellular and extracellular spaces have their largest conductivity parallel to the fibers. However, J_i will be rotated toward the fiber direction more than J_e , because of the greater anisotropy in the intracellular space, so the current loop will still exist. Assuming $g_L = g_T$ allows us to separate effects arising specifically because of unequal anisotropy ratios ($e \neq 0$) from effects arising because of the overall anisotropy of the tissue ($g_L \neq g_T$).

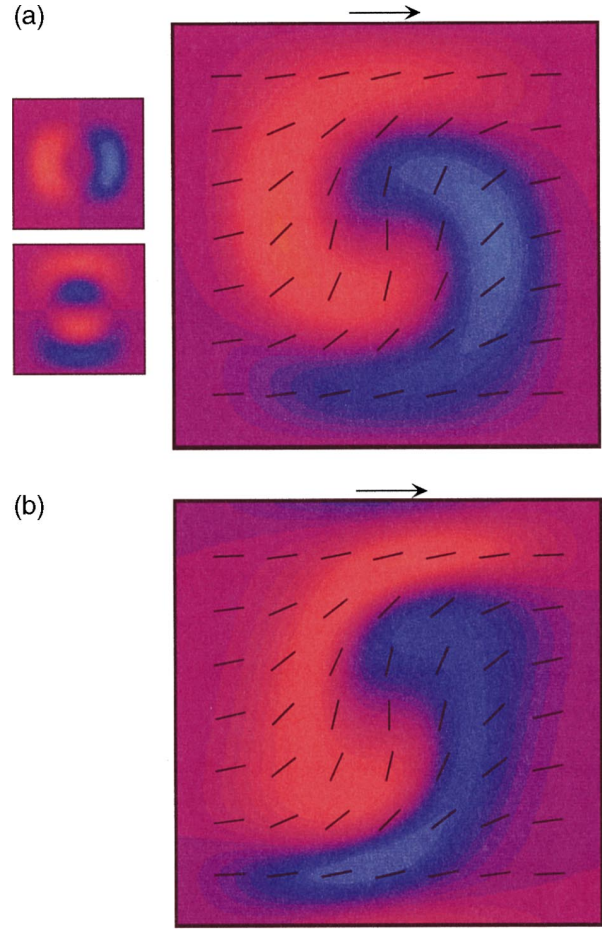


FIG. 6. (Color) The transmembrane potential as a function of x (horizontal) and y (vertical) (a) determined analytically using the approximate expression, and (b) computed numerically using the full bidomain model. The fiber geometry is given by $\theta(x,y) = \pi/2 \cos^2(\pi x/D) \cos^2(\pi y/D)$, and the local fiber direction is indicated by the line segments. A 20×20 mm² region of tissue is shown, with the origin at the center. The arrows indicate that the electric field points to the right (x direction). The parameters used in this calculation are $E_0 = 500$ V/m, $\phi = 0$, $\lambda_L = 0.434$ mm, $\lambda_T = 0.174$ mm, $\alpha = 1$, $e = 0.75$, and $D = 20$ mm. The two small panels on the left indicate the separate contributions of the two mechanisms. The color bar is the same as in Fig. 2.

$$\theta(x,y) = \tan^{-1}\left(\frac{y}{x}\right) + \frac{3\pi}{4}, \quad (30)$$

implying that

$$\sin 2\theta = \frac{y^2 - x^2}{x^2 + y^2}, \quad (31)$$

$$\cos 2\theta = \frac{2xy}{x^2 + y^2}, \quad (32)$$

$$\frac{\partial \theta}{\partial x} = -\frac{y}{x^2 + y^2}, \quad (33)$$

and

TABLE I. Bidomain parameters.

g_{iL}	0.1863 S/m
g_{iT}	0.0186 S/m
g_{eL}	0.1863 S/m
g_{eT}	0.0745 S/m
β	$0.3 \mu\text{m}^{-1}$
G_m	1.65 S/m^2

$$\frac{\partial \theta}{\partial y} = \frac{x}{x^2 + y^2}. \quad (34)$$

The resulting expression for V_m is

$$V_m = eE_0\lambda_L^2 \frac{1}{(x^2 + y^2)} [-\cos \phi y + \sin \phi x]. \quad (35)$$

The transmembrane potential produced by an electric field in the x direction is shown in Fig. 5. The polarization gets very large near the origin, because the fibers are spiraling into a singular point where the fiber direction changes dramatically over short distances. In this example, the fiber orientation changes in both the x and y directions, so that both mechanisms described in Fig. 4 contribute to the transmembrane potential. The two smaller panels to the left in Fig. 5 are the separate contributions of the two mechanisms, with the upper panel corresponding to the first mechanism, and the lower panel to the second.

IV. COMPARISON OF ANALYTICAL AND NUMERICAL CALCULATIONS

We have made several assumptions when deriving the approximate analytical solution given by Eq. (21). In particular, we assumed that we could retain only the first order terms in the expansion in powers of e , that the fiber orientation changed gradually enough that we could neglect the first two terms on the left-hand side of Eq. (18), and that the electric field is uniform, which can only be true in the case of $g_L = g_T$. In order to see how valid these assumptions are, we can calculate $V_m(x, y)$ numerically without these assumptions, and compare it to the expression in Eq. (21). One difficulty that arises is the influence of the boundary. When myocardial fibers approach a sealed boundary at an angle, a transmembrane potential is induced in the presence of an electric field [11]. We wish to exclude such boundary-induced membrane polarization from our analysis. The easiest way to avoid such boundary artifacts is to choose a fiber geometry such that the fibers are always parallel or perpendicular to the boundaries [6].

One simple fiber orientation that is zero at the tissue boundaries ($x = \pm D/2$ and $y = \pm D/2$) is

$$\theta(x, y) = \frac{\pi}{2} \cos^2\left(\pi \frac{x}{D}\right) \cos^2\left(\pi \frac{y}{D}\right), \quad (36)$$

shown in Fig. 1. When an electric field is in the x direction, it induces depolarization on the left and hyperpolarization on

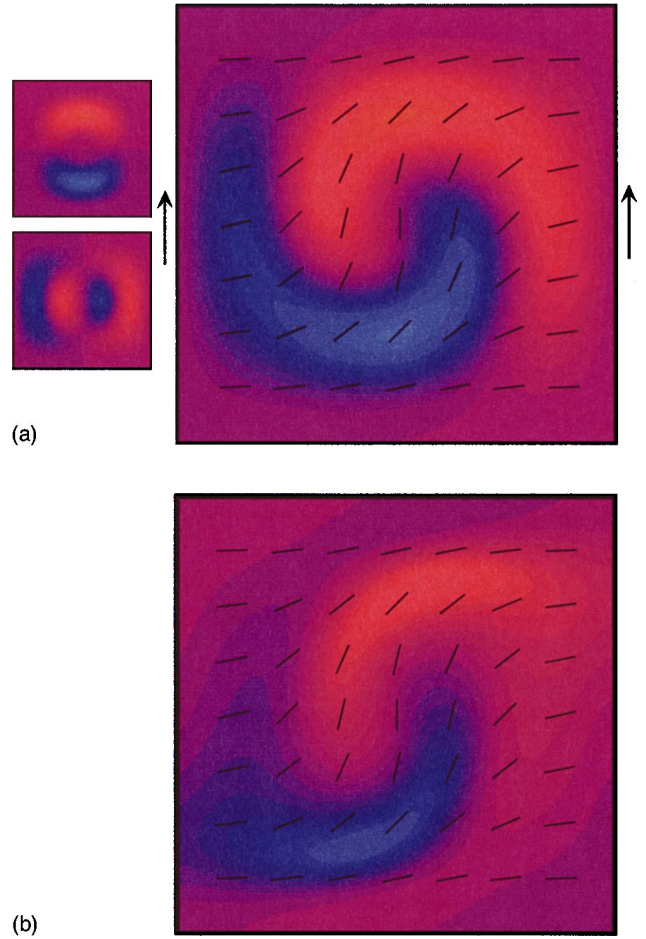


FIG. 7. (Color) The transmembrane potential as a function of x (horizontal) and y (vertical) (a) determined analytically using the approximate expression, and (b) computed numerically using the full bidomain model. The fiber geometry is given by $\theta(x, y) = \pi/2 \cos^2(\pi x/D) \cos^2(\pi y/D)$, and the local fiber direction is indicated by the line segments. A $20 \times 20 \text{ mm}^2$ region of tissue is shown, with the origin at the center. The arrows indicate that the electric field points up (y direction). The parameters used in this calculation are $E_0 = 500 \text{ V/m}$, $\phi = \pi/2$, $\lambda_L = 0.434 \text{ mm}$, $\lambda_T = 0.174 \text{ mm}$, $\alpha = 1$, $e = 0.75$, and $D = 20 \text{ mm}$. The two small panels on the left indicate the separate contributions of the two mechanisms. The color bar is the same as in Fig. 2.

the right by the first mechanism [Fig. 6(a), small top panel]. It also induces a more complicated distribution of hyperpolarization-depolarization-hyperpolarization-depolarization in the y direction by the second mechanism [Fig. 6(a), small bottom panel]. When these two contributions are added together, we obtain a spiral-like distribution of transmembrane potential [Fig. 6(a)].

We compare the result in Fig. 6(a) to the numerically calculated transmembrane potential using the full bidomain model, shown in Fig. 6(b). The bidomain equations were solved using a finite difference method described previously [13], using the parameters given in Table I. The space step was 0.1 mm , compared to a length constant parallel to the fibers of 0.43 mm . A grid of 201 by 201 nodes implies a tissue sheet $D = 20 \text{ mm}$ on each side. The boundary condi-

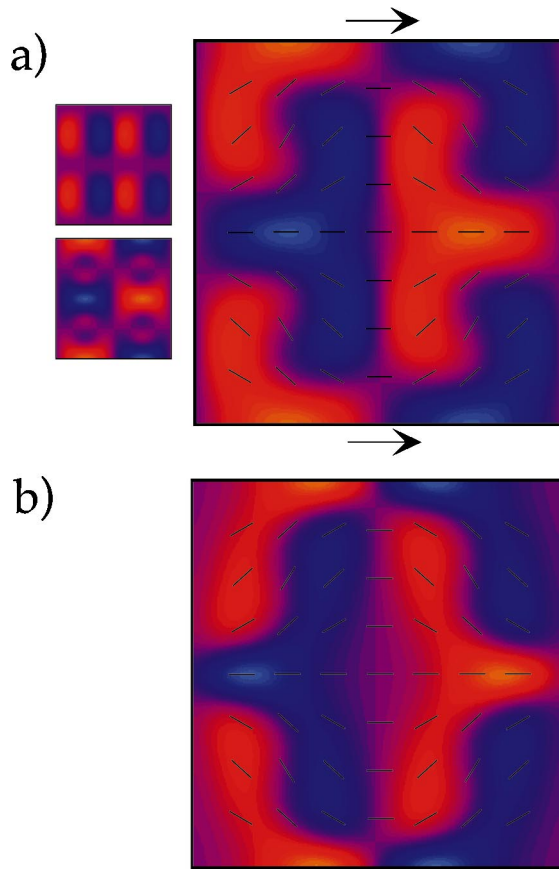


FIG. 8. (Color) The transmembrane potential as a function of x (horizontal) and y (vertical) (a) determined analytically using the approximate expression, and (b) computed numerically using the full bidomain model. The fiber geometry is given by $\theta(x,y) = -\sin(2\pi x/D)\sin(2\pi y/D)$, and the local fiber direction is indicated by the line segments. A 20×20 mm² region of tissue is shown, with the origin at the center. The arrows indicate that the electric field points to the right (x direction). The parameters used in this calculation are $E_0 = 500$ V/m, $\phi = 0$, $\lambda_L = 0.434$ mm, $\lambda_T = 0.174$ mm, $\alpha = 1$, $e = 0.75$, and $D = 20$ mm. The two small panels on the left indicate the separate contributions of the two mechanisms. The color bar is the same as in Fig. 2.

tions at the edge of the tissue are

$$\frac{\partial V_e}{\partial n} = 0 \quad (37a)$$

on sides parallel to the electric field,

$$V_e = \pm 5 \text{ V} \quad (37b)$$

on sides perpendicular to the electric field, and

$$\frac{\partial V_m}{\partial n} = 0. \quad (38)$$

The boundary condition for V_m implies that the normal components of V_e and V_i are the same, and ensures that there are no large boundary artifacts that would interfere with our

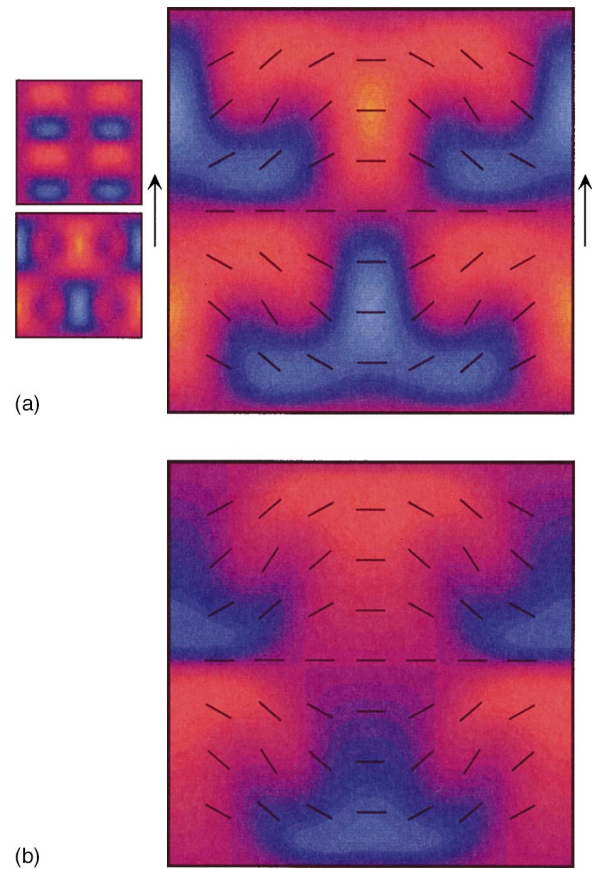


FIG. 9. (Color) The transmembrane potential as a function of x (horizontal) and y (vertical) (a) determined analytically using the approximate expression, and (b) computed numerically using the full bidomain model. The fiber geometry is given by $\theta(x,y) = -\sin(2\pi x/D)\sin(2\pi y/D)$, and the local fiber direction is indicated by the line segments. A 20×20 mm² region of tissue is shown, with the origin at the center. The arrows indicate that the electric field points up (y direction). The parameters used in this calculation are $E_0 = 500$ V/m, $\phi = \pi/2$, $\lambda_L = 0.434$ mm, $\lambda_T = 0.174$ mm, $\alpha = 1$, $e = 0.75$, and $D = 20$ mm. The two small panels on the left indicate the separate contributions of the two mechanisms. The color bar is the same as in Fig. 2.

study of far-field stimulation. The strength of the electric field, E_0 , is 500 V/m, and it is applied in either the x or y direction.

The analytical and numerical transmembrane potential distributions differ quantitatively, but have the same general qualitative form, implying that the analytical equations do not determine $V_m(x,y)$ accurately, but do provide an intuitive understanding of the V_m distribution and the underlying mechanisms that give rise to it. Figure 7 compares the analytical and numerical $V_m(x,y)$ for an electric field in the y direction.

A second example is shown in Fig. 8 for the fiber distribution

$$\theta(x,y) = -\sin\left(2\pi\frac{x}{D}\right)\sin\left(2\pi\frac{y}{D}\right)$$

with the electric field in the x direction. Figure 9 shows the

same fiber geometry with the electric field in the y direction. Again, quantitative differences exist between the analytic and numerical calculations, but the qualitative transmembrane potential distributions are the same.

V. DISCUSSION

The main result of our paper, exhibited in Fig. 4, is that two different mechanisms can induce polarization in cardiac tissue with curving fibers. The first, which applies when the fiber orientation changes along the direction of the electric field, arises as current redistributes from the intracellular space (favored when E is parallel to fibers) to the extracellular space (favored when E is perpendicular to fibers). The second, which applies when the fiber orientation changes perpendicularly to the direction of the electric field, arises because J_i and J_e are not parallel to E or to each other when the fibers are oriented obliquely. This provides a current loop through the intracellular space in one direction and back through the extracellular space in the opposite direction. Where these current loops end, the current must cross the membrane, thereby polarizing the tissue. Both mechanisms require unequal anisotropy ratios.

We are not the first to derive an approximate analytical solution of V_m for fiber curvature. Sobie *et al.* [9] proposed a “generalized activating function” that predicts regions of tissue polarization. Yet, the model of Sobie *et al.* did not emphasize the essential role of unequal anisotropy ratios. Our analytical solution suggests a similar “activating function,” but one that highlights the role of unequal anisotropy ratios. In addition, the model of Sobie *et al.* [9] did not go so far as to define their activating function in terms of the derivative of the fiber angle, θ , as ours does. Therefore, they were not able to qualitatively predict effects of the electric field applied to curving fibers and could not provide the same insight into the mechanisms behind the polarization that we obtained.

There are certain limitations to our approximation that could have affected our results. We assume that a first order approximation in our expansion of the small parameter e is sufficient, that the fiber curvature is small enough so the terms on the left-hand side of Eq. (18) can be ignored, and that the electric field is uniform. However, the polarization in

the tissue occurred in the same places in both the numerical calculation using the full bidomain model and the analytical calculation using an approximate model. Using more realistic fiber geometries may be a way to test our model further by comparing it with experimental data.

Two other possible mechanisms for electric field stimulation of cardiac tissue are macroscopic inhomogeneities and the sawtooth potential. A simple scaling comparison of the maximum transmembrane potential amplitude, $V_{m,\max}$, can be made between our results and the effects of these two mechanisms. Assuming that the electric field is in the direction of the fibers, macroscopic inhomogeneities can be represented by multiplying the electric field times the length constant, $V_{m,\max}=E\lambda$, and the sawtooth potential can be approximated by multiplying the electric field by the length of a myocardial cell, $V_{m,\max}=Ea$ [14]. For our fiber curvature solution, $V_{m,\max}$ can be approximated from Eq. (19) by $eE\lambda^2/L$, where L is a characteristic distance over which the fibers curve. The ratio of the $V_{m,\max}$ from macroscopic inhomogeneities to that from fiber curvature is $E\lambda/(eE\lambda^2/L)=L/e\lambda$. This ratio implies that inhomogeneities will dominate fiber curvature unless the fibers curve over a distance comparable to the length constant. The ratio of the $V_{m,\max}$ from the sawtooth potential to fiber curvature is $Ea/(eE\lambda^2/L)=(aL/e\lambda^2)$. The cell length a is much less than λ , but the distance over which fibers curve, L , is generally much greater than λ . Thus the ratio $aL/e\lambda^2$ is on the order of 1, so we can reach no conclusion about the dominant mechanism from this simple analysis.

We opened this manuscript by challenging the reader to predict qualitatively the transmembrane potential distribution for the fiber geometry shown in Fig. 1. The correct prediction is the spiral shape distribution of V_m shown in Fig. 6. The two mechanisms described in Fig. 4 are the key to making such predictions and to understanding membrane polarization caused by fiber curvature in cardiac tissue.

ACKNOWLEDGMENTS

This work was supported by grants from the National Institutes of Health (RO1 HL57207) and the American Heart Association—Midwest Affiliate.

-
- [1] B. J. Roth and W. Krassowska, *Chaos* **8**, 204 (1998).
 - [2] N. A. Trayanova, B. J. Roth, and L. J. Malden, *IEEE Trans. Biomed. Eng.* **40**, 899–908 (1993).
 - [3] E. Entcheva, N. A. Trayanova, and F. J. Claydon, *IEEE Trans. Biomed. Eng.* **46**, 260 (1999).
 - [4] N. Trayanova and K. Skouibine, *J. Electrocardiol.* **31**, 23 (1998).
 - [5] K. Skouibine, N. Trayanova, and P. Moore, *J. Cardiovasc. Electrophysiol.* **11**, 785 (2000).
 - [6] A. E. Lindblom, F. Aguel, and N. Trayanova, *J. Cardiovasc. Electrophysiol.* **12**, 946 (2001).
 - [7] C. S. Henriquez, *Crit. Rev. Biomed. Eng.* **21**, 1 (1993).
 - [8] B. J. Roth, *IEEE Trans. Biomed. Eng.* **44**, 326 (1997).
 - [9] E. A. Sobie, R. C. Susil, and L. Tung, *Biophys. J.* **73**, 1410 (1997).
 - [10] B. J. Roth, *Phys. Rev. E* **55**, 1819 (1997).
 - [11] B. J. Roth, *Med. Biol. Eng. Comput.* **37**, 523 (1999).
 - [12] B. J. Roth, W.-Q. Guo, and J. P. Wikswo, Jr., *Math. Biosci.* **88**, 191 (1988).
 - [13] B. J. Roth, *Circ. Res.* **68**, 162 (1991).
 - [14] B. J. Roth, *Crit. Rev. Biomed. Eng.* **22**, 253 (1995).